Journal of The Electrochemical Society, **161** (3) A290-A301 (2014)
0013-4651/2014/161(3)/A290/12/$31.00 © The Electrochemical Society

Mitigation of Layered to Spinel Conversion of a Li-Rich Layered Metal Oxide Cathode Material for Li-Ion Batteries

Mehmet Nurullah Ates,[a,b,*] Qingying Jia,[a] Ankita Shah,[b] Ahmed Busnaina,[b,] Sanjeev Mukerjee,[a,***] and K. M. Abraham[a,b,***,z]**

[a]*Center for Renewable Energy Technology, Department of Chemistry and Chemical Biology, Northeastern University, Boston, Massachusetts 02115, USA*
[b]*NSF Center for High-rate Nanomanufacturing, Northeastern University, Boston, Massachusetts 02115, USA*

We have prepared the Li-rich layered NMC composite cathode material of the composition $0.3Li_2MnO_3 0.7LiMn_{0.33}Ni_{0.33}Co_{0.33}O_2$, (NMC) with 5 wt% Na doping. The latter material with composition of $0.3Li_2MnO_3.0.7Li_{0.97}Na_{0.03}Mn_{0.33}Ni_{0.33}Co_{0.33}O_2$, synthesized as 200–300 nm size particles, was compared to its counterpart without Na. The discharge rate capability of the Li-rich NMC was greatly improved at both room temperature and 50°C with the Na doping. The Na doped material exhibited significantly higher conductivity than its un-doped analog as evidenced by dc electronic conductivity data and impedance of Li cells. Charge/discharge cycling results of Li cells at 50°C indicated that the voltage decay of Li-rich NMC accompanied by a layer to spinel structural conversion was mitigated with Na doping. XRD analysis revealed that ionic exchange of Na occurs upon contact of the cathode material with the electrolyte and produces a volume expansion of the crystal lattice which triggers a favorable metal (probably Ni) migration to Li depleted regions during oxidation of Li_2MnO_3 in the first cycle. XANES data showed that Na doped NMC has better Ni reduction efficiency to provide higher rate capability. EXAFS data supported this conclusion by showing that in the case of Na doped NMC, the structure has larger crystal cage allowing for better metal migration into the Li depleted regions located in the layered unit cell of C2/m space group. XANES of Mn K-edge supported by pre-edge analysis also revealed that during charging of the electrode, the Na doped NMC was oxidized to a higher Mn valence state compared to its undoped counterpart.
 [DOI: 10.1149/2.040403jes]

Manuscript submitted October 2, 2013; revised manuscript received November 18, 2013. Published December 23, 2013. This was Paper 813 presented at the San Francisco, California, Meeting of the Society, October 27–November 1, 2013.

Lithium-ion batteries are indispensable for everyday life as power sources for laptops, cellphones, e-book readers, digital cameras, and a variety of other portable devices. A typical Li-ion battery is composed of graphite anode and a layered transition metal oxide cathode active material, exemplified by $LiCoO_2$, or one of its congeners obtained by substituting some of the Co with Ni and/or Mn. These cathode materials exhibit specific capacities in the 140–200 mAh/g range which limit the specific energy of Li-ion cells constructed with them and graphite anode to 200–250 Wh/kg. Another class of layered transition metal oxides exhibiting significantly higher Li intercalation capacities are the lithium-rich layered-layered composite oxides of the general formula $xLi_2MnO_3.(1-x)LiMO_2$ (M = Mn, Ni, Co), which have been reported to deliver 230–285 mAh/g, reaching nearly the theoretical 1e-/metal capacity[1–4] of the transition metal dioxide. During the first charging of these oxides, Li extraction from the $LiMO_2$ portion takes place between 3.5 and 4.3 V, followed by the extraction of Li_2O (as Li^+ and O_2) from the Li_2MnO_3 portion, along with some electrolyte decomposition, at potentials between 4.3 and 5 V. Such a charging process leads to the formation of the $xMnO_2.(1-x)MO_2$ cathode active material. A variety of composite oxides have been prepared by varying the nature of the metal in the $LiMO_2$ portion and with various Li_2MnO_3:$LiMO_2$ ratios. The first cycle charging of these materials is very crucial, as it determines the structural integrity between the Li_2MnO_3 and $LiMO_2$ layered-layered components. Prior work has revealed several deficiencies that must be addressed to make these materials practical. These include: i) oxygen generation in the first charge and the first cycle irreversible capacity loss[5] ii) layered to spinel conversion during long-term cycling[1] iii) low rate capability, attributed in part to low electronic conductivity[6]

In this paper we report on solutions to two of the aforementioned deficiencies of the lithium rich layered-layered composite oxides by substituting some of the Li with Na, most likely in the $LiMO_2$ portion of the $0.3Li_2MnO_3.0.7LiMn_{0.33}Ni_{0.33}Co_{0.33}O_2$ structure. We have found that substituting about 5 weight-percent of Li with Na in this composite oxide increases: i) its rate capability and ii) mitigates the layered to spinel structural conversion during long-term cycling. We have come to this conclusion from detailed analysis of the structure and elemental composition of the Na doped Li-rich layered-layered NMC composite oxide by means of X-ray diffraction (XRD), X-ray absorption spectroscopy (XAS), and scanning electron microscopy (SEM) coupled with energy dispersive X-ray analysis (EDAX). These data are complemented with electrochemical impedance and galvanostatic charge-discharge cycling results for Li cells at room temperature and 50°C. The results reported here are expected to accelerate the full development of these high capacity positive electrode materials for Li-ion batteries.

Experimental

Lithium-rich cathode materials of the composition, $0.3Li_2MnO_3.0.7LiMn_{0.33}Ni_{0.33}Co_{0.33}O_2$, denoted as R-NMC, and its Na doped analog denoted as Na-NMC formulated as $0.3Li_2MnO_3.0.7Li_{0.97}Na_{0.03}Mn_{0.33}Ni_{0.33}Co_{0.33}O_2$, were synthesized using a co-precipitation procedure followed by high temperature sintering. Starting from the nitrate salts of manganese, nickel and cobalt, [$(Mn(NO_3)_2.4H_2O$, $Ni(NO_3)_2.6H_2O$, and $Co(NO_3)_2.6H_2O$)], co-precipitation of the mixed metal hydroxides was carried out under a mildly alkaline condition. The pH of solution was maintained at 11-12 (as monitored by SympHony pH meter, model SP70P). The precipitated manganese, nickel and cobalt hydroxides were filtered, washed in copious deionized water at least twice. The precipitate was dried in a vacuum oven and then intimately mixed with an appropriate amount of $LiOH.H_2O$ and pelletized. The 5 wt% Na doped NMC was synthesized using the same procedure except for replacing 5 wt% $LiOH.H_2O$ with Na_2CO_3. The pelletized powders were then heat-treated in atmospheric air for: i) 3 hours at 480°C, followed by ii) 3 hours at 900°C. A 3 wt% excess of $LiOH.H_2O$ was used to compensate for possible lithium evaporation loss during the sintering.

To prepare a Ni^{4+} reference material for XAS experiments, $LiNi_{0.85}Co_{0.15}O_2$ was synthesized via solid state reaction from appropriate amounts of $LiOH.H_2O$, $Ni(Ac)_2.4H_2O$ and $Co(Ac)_2.4H_2O$. The precursor mixture was thoroughly mixed and fired at 630°C for 8 hours and the powder was ground, pelletized and fired at 750°C for another 16 hours. Charging of this material in a Li cell to 5.1 V produced the Ni^{4+} reference material.[7]

X-ray diffraction spectra were recorded over the 2θ range of 10–80 degrees with a Rigaku Ultima IV diffractometer using CuKα radiation.

*Electrochemical Society Student Member.
**Electrochemical Society Active Member.
***Electrochemical Society Fellow.
zE-mail:kmabraham@comcast.net

Unit cell constants of the synthesized compounds were refined with PDXL software program provided by Rigaku Corporation. XRD unit cell visualizations were run via VESTA software.[8]

Particle morphology measurement and elemental analysis were performed with a Hitachi S-4800 Field emission scanning electron microscope (SEM) combined with its energy dispersive X-ray spectroscopy (EDAX) module.

Impedance measurements of Li cells utilizing the cathode materials were performed in the range of 100 kHz to 10 mHz with a 10 mV potentiostatic sine wave amplitude on a Voltalab PGZ402 model instrument in order to evaluate and compare the impedance responses of the various materials. Some measurements were made in a three-electrode cell with Li both as counter and reference electrodes.

Galvanostatic charge/discharge cycling was performed on an Arbin Instruments BT2000 model cycler. Pressed cathode electrodes were prepared from 80 weight percent (w/o) active material, 10 w/o Super-P conductive carbon (TimCal), and 10 w/o polyvinylideneflouride (PVDF). The slurry of the electrode mix made with N-methyl-2-pyrrolidone (NMP) was cast on an aluminum foil (with doctor blade to control thickness) and dried overnight at 100°C under vacuum. The electrodes had typical active material loading of about 5 mg/cm^2. Coin cells were assembled in an argon-filled glove box and filled with 1 M $LiPF_6$ /1:1.2 EC/DMC electrolyte. A porous polypropylene membrane separated the active positive electrode and lithium foil negative electrode in the cell. Some cell cycling experiments were also conducted in Swagelok Li half-cells referred to as 'T-cells' in order to allow us to disassemble the cell after the experiments and retrieve the electrodes for analysis. These conventional test cells shaped like a 'T' have been routinely used for Li-ion battery materials characterization.[9] The T shape allows for the use of a Li-reference electrode as well as the anode and cathode in the test cell. The cells were cycled at room temperature and 50°C. The theoretical capacity of R-NCM composite compound was taken as 280 mAh/g.

X-ray absorption spectroscopy measurements were performed in the transmission mode at the Ni, Co and Mn K edge at beam line X-3A of the National Synchrotron Light Source at Brookhaven National Laboratory. Electrodes from the T-cells and coin cells, cycled at low rates (C/20), extracted and sealed with Kapton tape and stored in glass vials, were taped with Teflon tape and packed in moisture impermeable aluminized bags under argon to avoid any possible oxidation during transportation to the Light source. The data was processed and fitted using the Athena and Artemis software programs. Scans were calibrated, aligned and normalized with background removed using the IFEFFIT suite.[10,11]

The dc electronic conductivity measurements were made using pellets of the oxides pressed at 5000 psi. The pellets, 0.95 cm in diameter and 0.23 cm thick with a consistent density of about 2 g/cm^3, were coated with conductive graphite and housed between copper plates in a delrin casing. The dc current-voltage data for the electrodes were obtained using an Autolab potentiostat. Pelletized powders of both Na-NMC and R-NMC samples were mounted on a specially designed delrin case and galvanostatic excitation current was maintained for 50 seconds at room temperature yielding a constant voltage response from which resistance (R) was extracted from the I-V curve based on Ohm's law. Resistivity (δ) was determined using the equation;

$$\delta = RA/L$$

where, A is the pellet area and L is its thickness. 1/ δ yielded dc electronic conductivity for each compound.

Results and Discussion

The ramifications of Na substitution have been studied both experimentally and theoretically using a variety of cathode active materials including $LiMn_{1-y}Ni_yO_2$, $LiFePO_4$ and $LiVPO_4F$.[12–16] Ceder et al. found that $Na_{0.5}MO_2$ cathode materials have more robust structures than $Li_{0.5}MO_2$ by demonstrating through computational methods that layered to spinel transformation is not observed in the Na compound.[17] Also, while $NaVO_2$, belonging to the rhombohedral phase, remains structurally intact during cycling,[18] layered (R3m SG) $LiVO_2$ transforms to the spinel phase during very early stages of cycling.[19] Delmas et al reported the high conductivity of $Na_{0.5}CoO_2$ that has hexagonal P63/mmc SG by demonstrating metallic-type feature for $Na_{0.5}CoO_2$.[20] A very recent paper confirmed Na_xCoO_2 have metallic conductivity which leads to rapid Na^+ intercalation in this material up to the 400 C-rates with only 15.4% capacity fade after 100 cycles.[21] Recently, Johnson et al. reported that lithium rich layered-spinel cathode active material can be synthesized through ion-exchange reaction aiming to minimize disorder in $LiMO_2$ layers. However, their conclusion was not sufficient to elucidate the role of Na in the structure during cycling.[22] During the manuscript preparation we came across a very recent paper with contents[23] similar to ours. We have found that electrochemical performance of the lithium rich layered-layered metal oxide cathode material $0.3Li_2MnO_30.7LiMn_{0.33}Ni_{0.33}Co_{0.33}O_2$ can be significantly improved by substituting Li with 5 wt% Na in the $LiMO_2$ portion of the composite. We present here detailed structural analysis of the new cathode material through scanning electron microscopy (SEM) combined with EDAX, X-ray diffraction (XRD), and X-ray absorption spectroscopy (XAS). These results are complemented by electrochemical impedance and galvanostatic charge-discharge cycling data for Li cells built with these cathode materials at room temperature and 50°C.

Lithium cell cycling data.— Electrochemical cycling and rate capability data displayed in Figures 1a and 1b, respectively, clearly

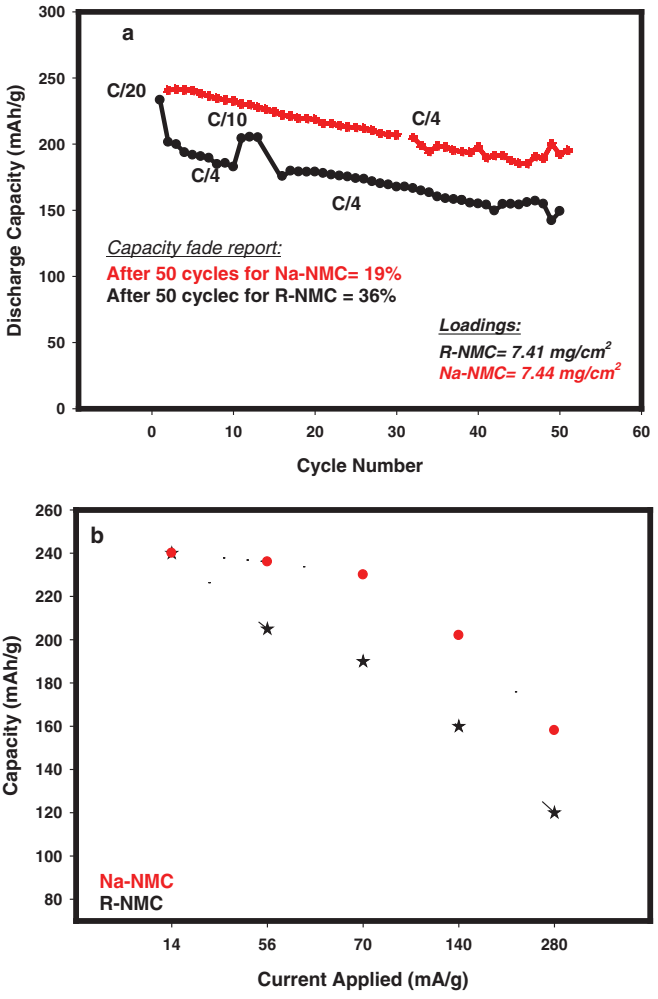

Figure 1. a) Cycling behavior of R-NMC and Na-NMC at different discharge rates between 2 and 4.9 V at room temperature. Charging rates were set at C/20. b) Rate capabilities of R-NMC and Na-NMC composite cathodes at RT.

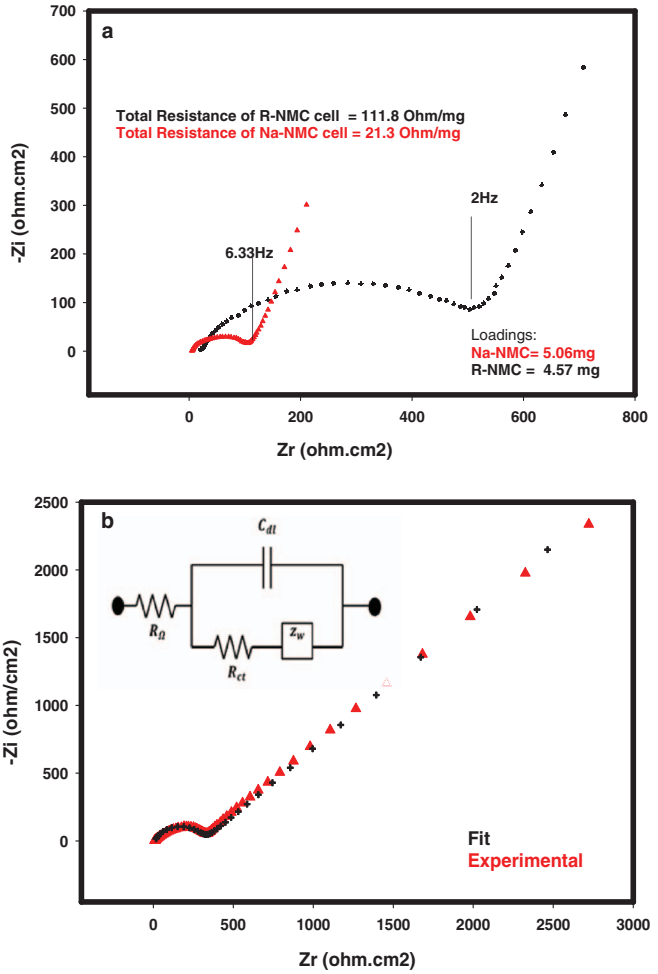

Figure 2. a) Nyquist plots of fresh cells of Na-NMC and R-NMC at room temperature; b) the experimental and fitted data along with the RC model used for the fit.

demonstrate that Na-NMC has better rate capabilities than R-NMC, although both materials showed similar capacity fade rate due to a variety of issues such as cell internal resistance, problems related to the Li anode etc. This prompted us to perform several experiments to understand the differences between the Na-doped and un-doped materials. The discharge capacity of R-NMC at C/4 was around 160 mAh/g, similar to reported values,[24] while Na-NMC exhibited 200 mAh/g at the same discharge rate as shown in Figure 1a. In order to shed light on the improved behavior of the Na doped material, we measured AC impedances of Li cells, and determined the dc conductivity of pressed pellets. Figure 2a shows Nyquist plots of Na-NMC and R-NMC at open circuit voltages (OCV) at room temperature, right after the Li half-cell was assembled using coin cell. We performed the same experiment in three-electrode T-cells with Li metal as anode and reference electrodes, and determined that the large difference between the impedances of the R-NMC and Na-NMC cells is associated with the cathode. The impedance, which is a sum of Re-ohmic, Rs-surface and Rct-charge transfer resistances, of the R-NMC cell is drastically decreased once 5 wt% Na is substituted for Li as can be seen from Figure 2a. The first term Re in the impedance spectrum falls at the highest frequency intercept from the origin and often is very small. The Rs and Rct can sometimes overlap especially if the cell was not cycled. This is true if one takes into consideration Rs which is mostly influenced by SEI formation, triggered largely by cycling. Since both materials are in the fresh condition when impedance was measured, we do not expect significant contribution from SEI formation. Thus, we believe that the semicircle is largely due to the charge transfer resistance Rct of the synthesized bulk materials that has different resistivity properties.

Similar improvement in charge transfer resistance was reported elsewhere for a different family of cathode active material, namely P2-Na_xCoO_2 ($\sigma > 10^3$ S/cm).[20,21] We used a simple Randles circuit for fitting the AC impedance data. The model used and the fitted data, which matches smoothly, are found in Figure 2b. The charge transfer resistance (R_{ct}) and double layer capacitance (C_{dl}) were found to be 310Ω and 10 μF, respectively.

To the best of our knowledge there has been no dc conductivity data reported to date for lithium rich layered-layered cathode active materials. We found dc conductivity for Na-NMC to be around 3.1×10^{-6} S/cm, while for R-NMC that was approximately 2.8×10^{-8} S/cm which suggests that the lower charge transfer resistance of Li/Na-NMC cells is probably associated with the higher electronic conductivity of the cathode.

Cycling behavior of the two materials from coin cells revealed lower capacity fade rate for Na-NMC cells. For example, the R-NMC cell was cycled 46 times at the C/4 discharge rate with a final capacity of 155 mAh/g, while the Na-NMC cell was cycled 51 times at C/4 with an end capacity of 195 mAh/g.

The layered to spinel metal oxide conversion.— We were particularly interested in finding out if Na doping mitigated the undesirable layered to spinel metal oxide conversion of the Li-rich NMC. Voltage decay as a result of this conversion during cycling is one of the

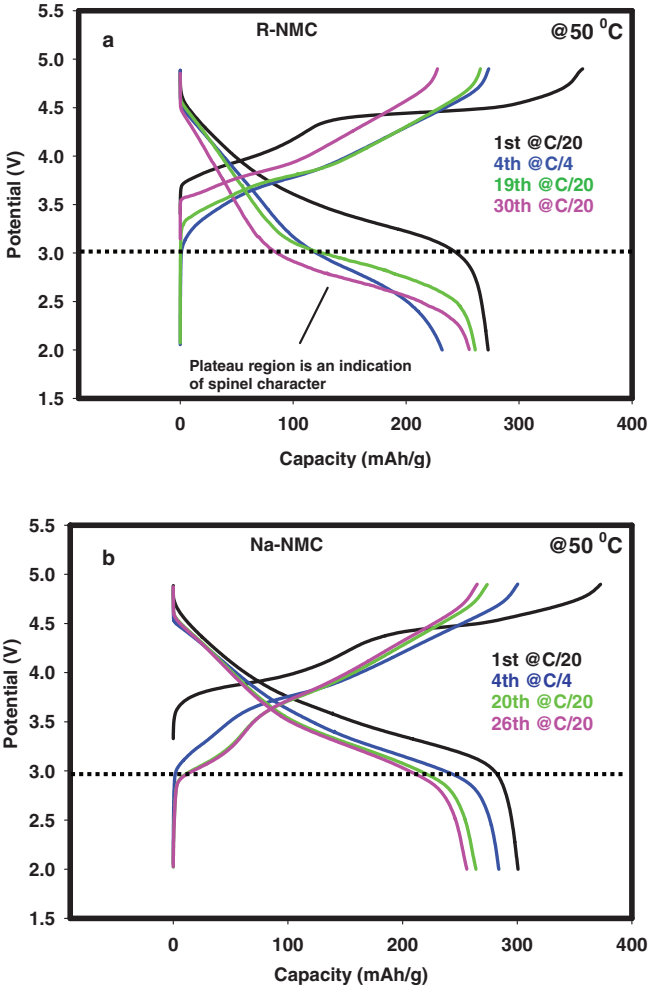

Figure 3. Charge-Discharge profiles of coin cells comprised of the cathodes; a-) R-NMC; b-) Na-NMC, at 50°C between 2 and 4.9 V.

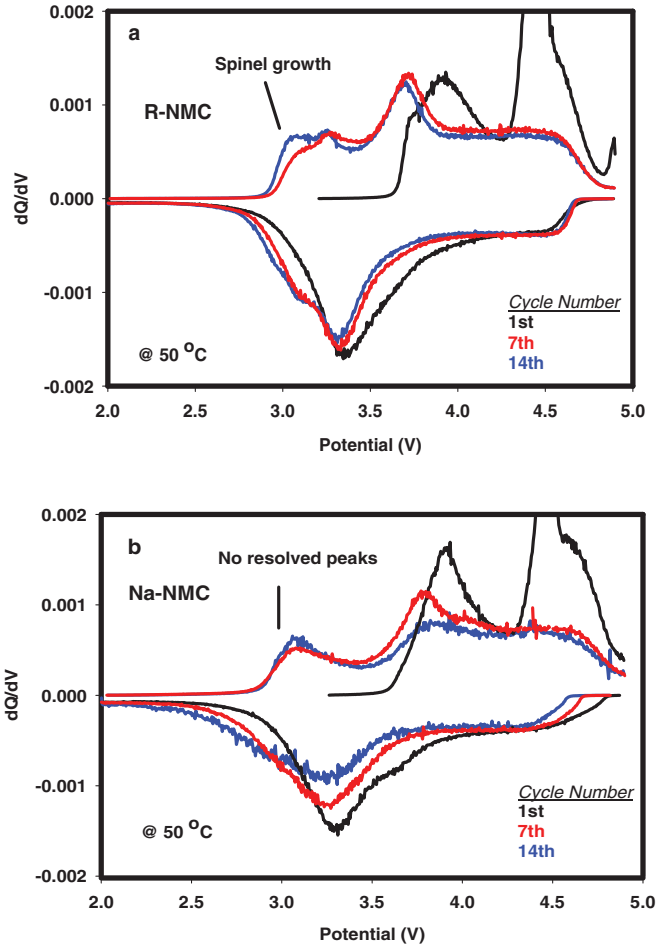

Figure 4. Derivative capacity plots (dQ/dV) of a) R-NMC b-) Na-NMC at 50°C between 2-4.9 V region.

major challenges for the lithium rich composite cathodes as reported by Thackeray et al.[1]

We elucidated the cycling behavior of both the Na-NMC and R-NMC cathodes at 50°C. It is believed that at higher temperatures, the layered to spinel metal oxide structural conversion of the Li-rich NMC is accelerated due to Mn^{2+} formation according to the disproportionation reaction shown below,[5]

$$2Mn^{3+} \rightarrow Mn^{2+} + Mn^{4+}$$

The formation of Mn^{2+} takes place through Jahn-Teller active[25] Mn^{3+} which is easier to decompose at higher temperatures.[4] Dissolved Mn^{2+} may also plate out on the anode and hinder further cycling. We studied the layered to spinel conversion of the two NMC materials through galvanostatic charging and discharging of coin cells at 50°C. In this experiment, each coin cell was weighed before and after the experiments to follow any electrolyte loss during the cycling. There was no weight change suggesting excellent seal integrity for the cells. Figure 3a and 3b show the charge/discharge voltage-capacity profiles of R-NMC and Na-NMC electrodes, respectively, at 50°C. Each figure includes an inset explaining the cycle number and the applied rate. In Figure 3a, for R-NMC, a clear voltage decay occurs with the voltage depressing to a plateau below 3 V. Several authors have attributed this behavior to[1,5] the layered to spinel conversion of the R-NMC. Interestingly, in Figure 3b, which depicts the cycling of Na-NMC, this behavior is inhibited. Furthermore, differential capacity (dQ/dV) plots shown in Figure 4a and 4b for R-NMC and Na-NMC, respectively demonstrates a clear spinel growth at ~ 3 V during the oxidation as cycling continues for R-NMC (Figure 4a) while it is absent in Figure 4b for Na-NMC. This behavior is another tell-tale indication of layered to spinel structural conversion in the composite cathodes.[1,25]

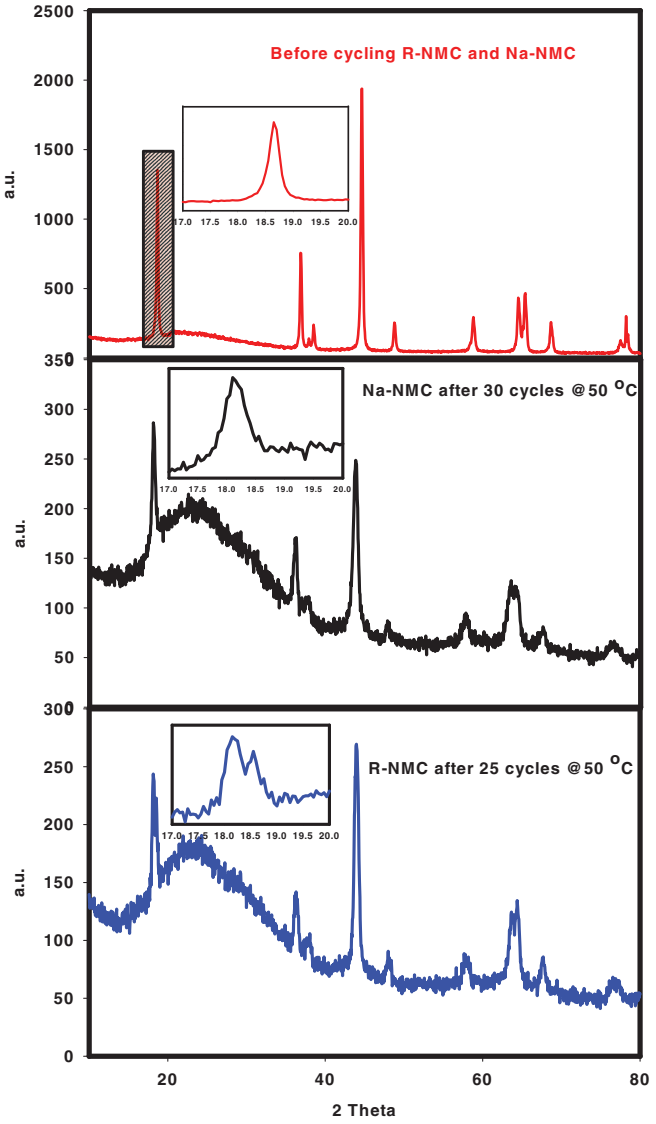

Figure 5. Ex situ XRD patterns before and after 30 and 25 cycles at 50°C of Na-NMC and R-NMC, respectively. Na-NMC and R-NMC before cycling have identical profiles.

These data affirm that Na doping is not just improving conductivity of the Li rich NMC but also mitigates the layered-spinel conversion which serve to improve its cycle life and rate capabilities.

XRD profiles of post discharge samples of both electrode materials provided further support to this conclusion. Figure 5 displays the XRD patterns of the NMC electrodes before and after many cycles (indicated in the inset of each figure) at 50°C. The Na-NMC exhibits a more robust structure by maintaining the symmetry of the (003) the peak, after 30 cycles at 50°C. On the other hand, after 25 cycles at 50°C, R-NMC reveals a broadened peak with a clear splitting of the (003) peak suggesting that the layered-spinel structural conversion took place in this metal oxide as revealed through charge-discharge cycling and dQ/dV profiles at 50°C. The peak splitting and broadening appeared in the (003) peak of R-NMC after cycling were previously attributed to the layered to spinel conversion feature by several groups.[26,27]

Sodium exchange with lithium in the electrolyte.— The small amount of Na (5 wt% relative to Li) doped into the lithium-rich composite cathode was expected to remain in the structure after cycling in the Li cells. However, EDAX evaluation of cycled cathodes showed that a good portion of the doped Na ionically exchanged with

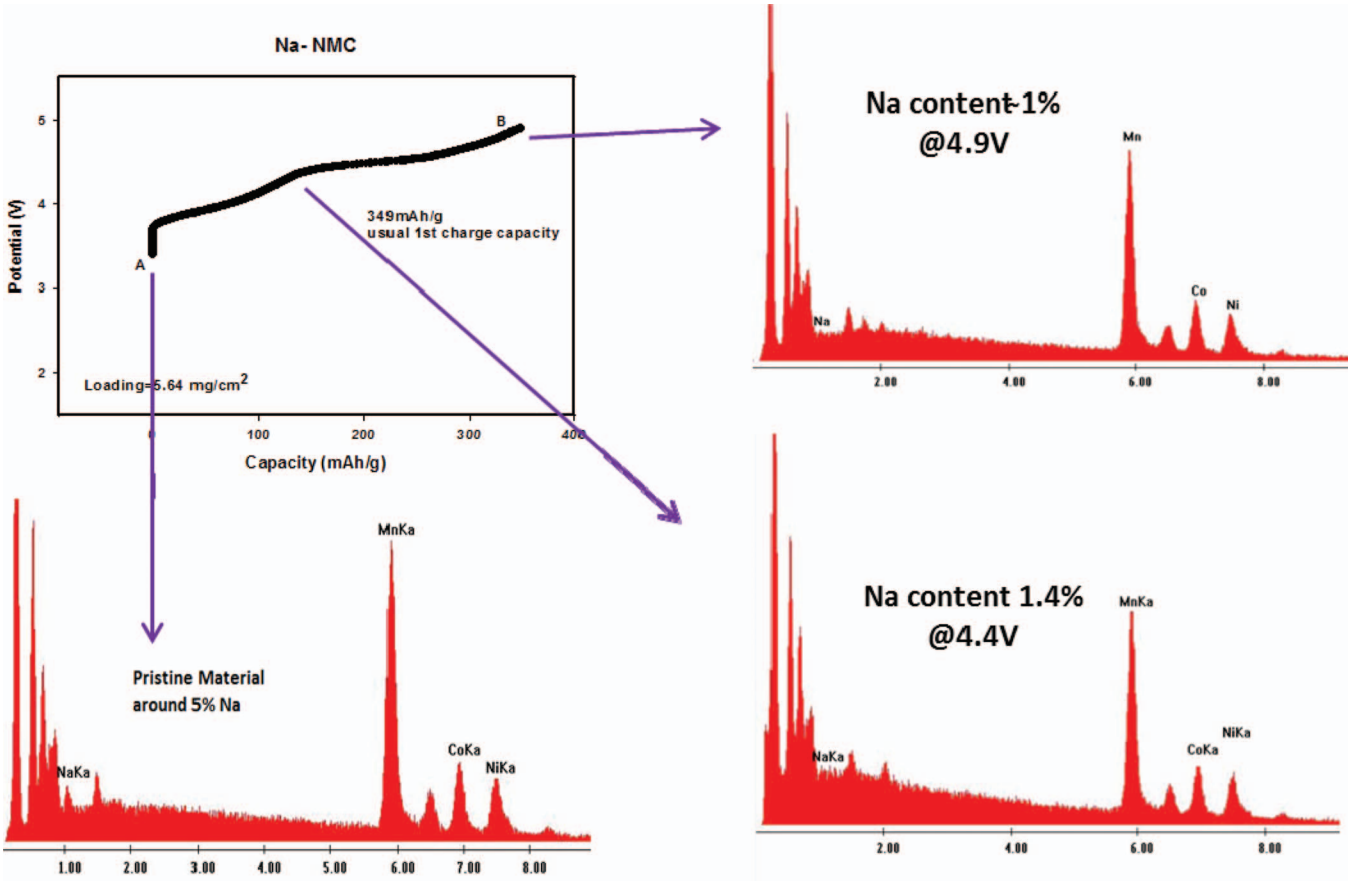

Figure 6. Evolution of EDAX profiles during the first charging cycle up to 4.9 V at room temperature of a Li/Na-NMC cell utilizing 1 M $LiPF_6$ /1:1.2 EC/DMC electrolyte. Excess of the electrolyte was employed in order for Na ions to be ionically exchanged efficiently in the T-cell.

the Li ions present in the electrolyte. EDAX evolution during the first charge to various potentials is depicted in Figure 6. This finding was complemented by an experiment in which cathode powder was stirred with the electrolyte overnight in a glass vial, and subsequently the amount of Na remained in the material was examined via EDAX. The amount of Na in the pristine cathode powders was 5 atomic percent before the stirring with the Li^+ electrolyte. However, after vigorously stirring in the 1 M $LiPF_6$/1:1.2 EC/DMC electrolyte overnight, the amount of Na in the cathode decreased to approximately 1% (as measured by EDAX) which suggested an ion-exchange reaction between the Na and Li ions. The EDAX profile pertaining to this experiment can be seen in Figure 7a. Both experiments demonstrated that after vigorous mixing of Na-NMC with Li^+ electrolyte or charging to 4.9 V, which requires 24h to reach that potential, approximately 1% Na still remains in the structure. Another experiment in which the Na doped material was stirred in the 1:1.2 EC/DMC solvent only (without the $LiPF_6$), the amount of Na did not change after stirring for 24 hours (Figure 7b) affirming that Na is not present in the compound as an impurity and that the Na and Li exchange occurs by ion swapping. We note that although EDAX technique is not a rigid way to determine the elemental composition; the data represent the average of many samples with runs on several segments of each sample, thereby providing unambiguous conclusions. We also performed dc electronic conductivity for Na-NMC material after stirring it with the Li^+ electrolyte for 4 days in order to determine the conductivity changes after a good amount of Na is exchanged with Li. There was a slight decrease in conductivity for Na-NMC (10^{-7} S/cm). The Na-NMC still possessed better conductivity than R-NMC. A comparison of conductivity values are given in Table I.

Since the Na present in the cathode is ionically exchanging with Li, the EIS profile could also change during cycling and/or with storage. In other words, the impedance of the cell may increase with time. Therefore, we performed another set of impedance experiments in which after assembling the cells, we waited overnight to allow exchange of Na with Li in Na-NMC. Figure 8 exhibits the Nyquist plot of the cells acquired after waiting overnight when the Na-NMC cell showed less resistance. It appears that even after removal of a significant portion of Na from the structure, the remaining 1% Na is sufficient to impart higher conductivity. Since Li ions have the highest ''charge to radius'' ratio among alkali metals, they form stronger covalent bonds with oxygen atoms than other alkali metals including Na.[28] Because of the tendency for lower covalency, Na increases the conductivity of the compound in which it is substituted for Li. Moreover, Na ions create larger unit cells (which will be discussed in connection with XRD analysis) causing better transition metal motions and/or migration thereby improving conductivity through correlated enhanced motion of electrons. This provides an explanation for the higher dc conductivity of Na-NMC. The ion exchange data together with X-ray diffraction and absorption spectroscopic information presented below, supported by electrochemical results, indicate that the exchange between the Na^+ in Na-NMC and the Li^+ in solution is a necessary step in order to produce the improved electrochemical behavior and crystal structural stabilization that mitigates the layered to spinel conversion in Li-rich NMC. It appears that these improvements of Na-NMC are accomplished through transition metal (most probably Ni^{3+}) migration to the vacancies created by the removal of the larger Na^+ in the crystal structure.

Crystal structure considerations.— The X-ray diffraction patterns of the Na-NMC and R-NMC materials are very similar as shown Figure 9. All the diffraction peaks can be indexed to a pseudo-trigonal unit cell with *R3m* symmetry. Specifically, the weak diffraction peaks

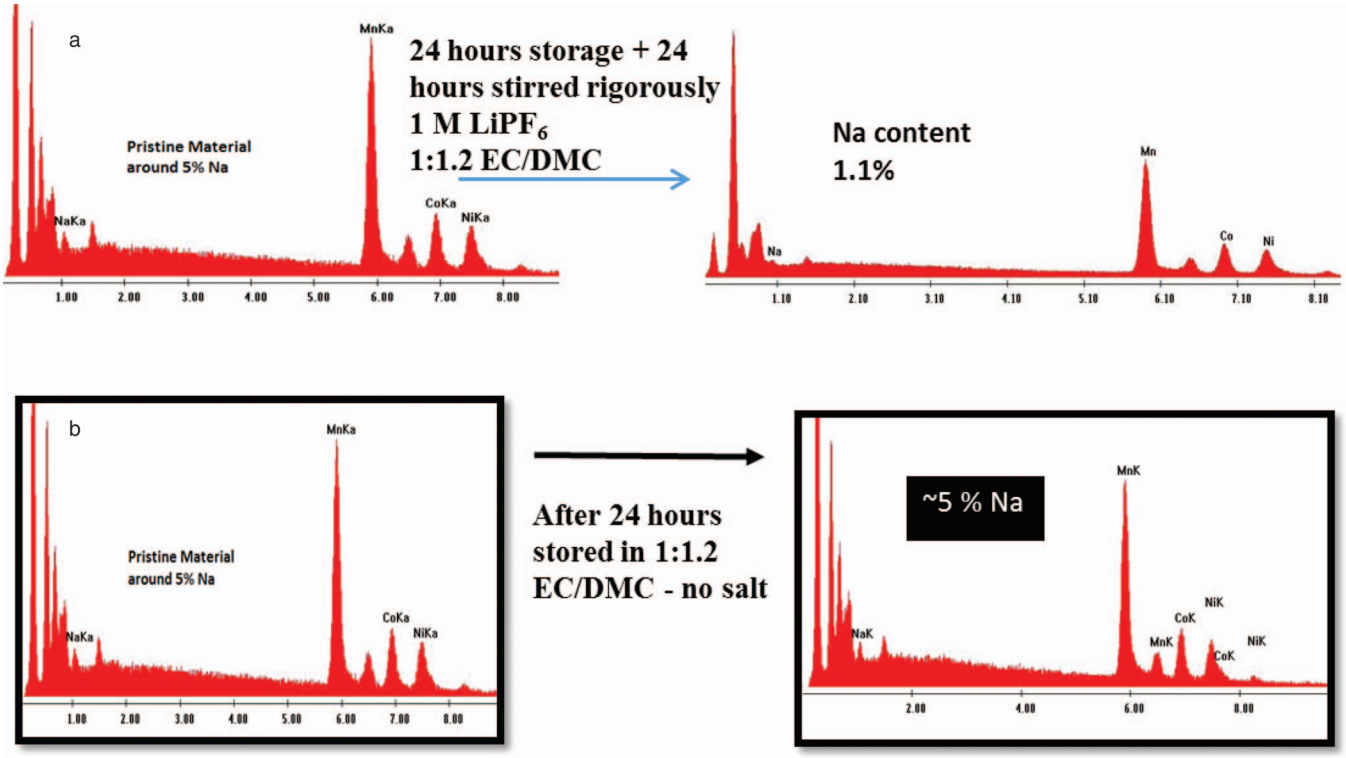

Figure 7. a) EDAX profiles of pristine Na-NMC and after 48 hours stored in 1 M $LiPF_6$ /1:1.2 EC/DMC treatment. b) EDAX profiles of 5% wt Na doped Li-rich NMC and after 24 hours stored in 1:1.2 EC/DMC mixture without $LiPF_6$ salt.

between 21° and 25° 2θ values are characteristic of the Li_2MnO_3 crystalline component in the integrated composite cathode structure as noted by others.[29,30] The peaks corresponding to Li_2MnO_3 is magnified in the inset of Figure 9 for each composite material supporting the view that the cathodes have similar amount of Li_2MnO_3. Moreover, the (006)/(012) and (018)/(110) doublets clearly indicate a highly ordered layered structure.[31] The former is located at around 39° and the latter is centered at 65°. The ratio of the intensities of the two major peaks I(003)/I(104) is a direct indication of cation mixing.[32,33] Na-NMC gave a I(003)/I(104) value of 1.288 whereas R-NMC cathode showed this value to be 1.114. The higher value of this ratio for Na-NMC than for R-NMC suggests that Na-NMC suppresses cation mixing[34] during sintering by introducing some Na atoms into the $LiMO_2$ lattice positions. This structural difference has a direct effect on the electrochemical performance of the cathodes.

In another investigation of XRD, we found that the concentration of $LiOH.H_2O$ used along with the metal salts play a significant role on the purity of the metal hydroxide precursors obtained during co-precipitation. When the amount of $LiOH.H_2O$ was 0.05M, the XRD patterns of the product contained the pattern for Hausmannite (Mn_3O_4) peaks which can be detrimental to the electrochemical performance of the battery.[35] However, if the amount of $LiOH.H_2O$ was 0.2M, the product did not show the Mn_3O_4 patterns. A morphological investigation from SEM attests to the nanometer size particles of the active materials as displayed in Figure 10 which includes a magnified image in the inset. Both Na doped and R-NMC powders revealed similar particle sizes and transition metal contents based on EDAX profiles presented in the inset of Figure 10. This figure also displays the EDAX profiles of both Na-NMC and R-NMC materials which clearly show Na peak for Na-NMC suggesting that Na doping is preserved after calcination at 900°C for 3 hours. In addition, mapping displayed in the inset of Figure 10 confirms the homogenous distribution of transition metals and Na atoms throughout the Na-NMC cathode.

Figure 11 displays the refined XRD patterns of R-NMC powders using two different target phases namely Li_2MnO_3 (S.G. C2/m) and $LiMO_2$ (S.G. R3m). By using the relative intensity ratio (RIR) technique we found that the fraction of each layered structure in the

Table I. Comparison of dc electronic conductivity values of Na-NMC, R-NMC, and Na-NMC stirred with typical electrolyte 4 days.

	Conductivity (S/cm)
R-NMC	2.8×10^{-8}
Na-NMC	3.1×10^{-6}
Na-NMC after stirring 4 days with 1 M $LiPF_6$ 1:2 EC/DMC	4.6×10^{-7}

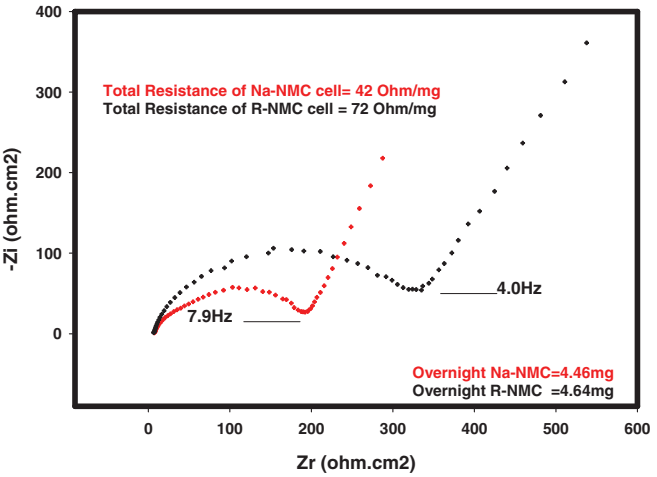

Figure 8. Nyquist plots of Li/ Na-NMC and R-NMC cells after overnight at room temperature.

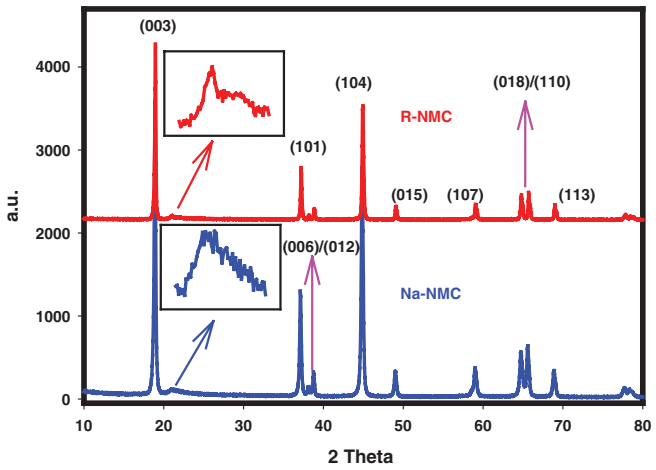

Figure 9. XRD patterns of: (blue) 5 wt% Na doped NMC; (red) regular NMC without dopant.

integrated composite cathode was around 78% of $LiMO_2$ and 22% of Li_2MnO_3. These values were identical for Na-NMC powders as well. The atomic coordinates for both phases were not further refined as well as stacking faults; however; the fraction values obtained is in the range of acceptable accuracy as reported in a study elsewhere.[36] We also examined the XRD patterns of Na-NMC powders after being stirred with the carbonate electrolyte for 24 hours and 48 hours. Refined unit cell parameters, which have acceptable accuracy, for pristine and treated samples are tabulated in Table II. From this data one can surmise that pristine Na-NMC has greater volume than R-NMC which is attributed to the larger ionic radius of doped Na. Furthermore, as the Na is ionically exchanged, the main unit cell difference is observed in the c direction (Table II) which advocates that doped Na is located most probably in the Li layers. It is to be noted that Li^+ (0.76A) has the closest ionic radius to Na^+ (1.02A). To visualize this feature, we illustrate the unit cells of each layered space groups in the composite material in Figure 12. After substituting the whole Li with Na in the $LiMO_2$ layers as shown in Figure 12c, there is a clear expansion in c direction which is expected due to the larger ionic radius of Na. The reason why we illustrate Na doping in the $LiMO_2$ (space group, R3m) portion, which has higher symmetry group than Li_2MnO_3 (space group C2/m), is that after the first charge, layered-layered composite cathode transforms into a single phase which is believed to be similar to $LiMO_2$.[5] In this structural model presented in Figure 12a we adopted an R3m-layered oxide unit cell where Mn, Ni and Co atoms partially occupy octahedral 3a sites with no specific ordering while Na and Li occupy octahedral 3b sites.[37] In addition, we observed a trend in which after electrolyte storage treatment, for 24h

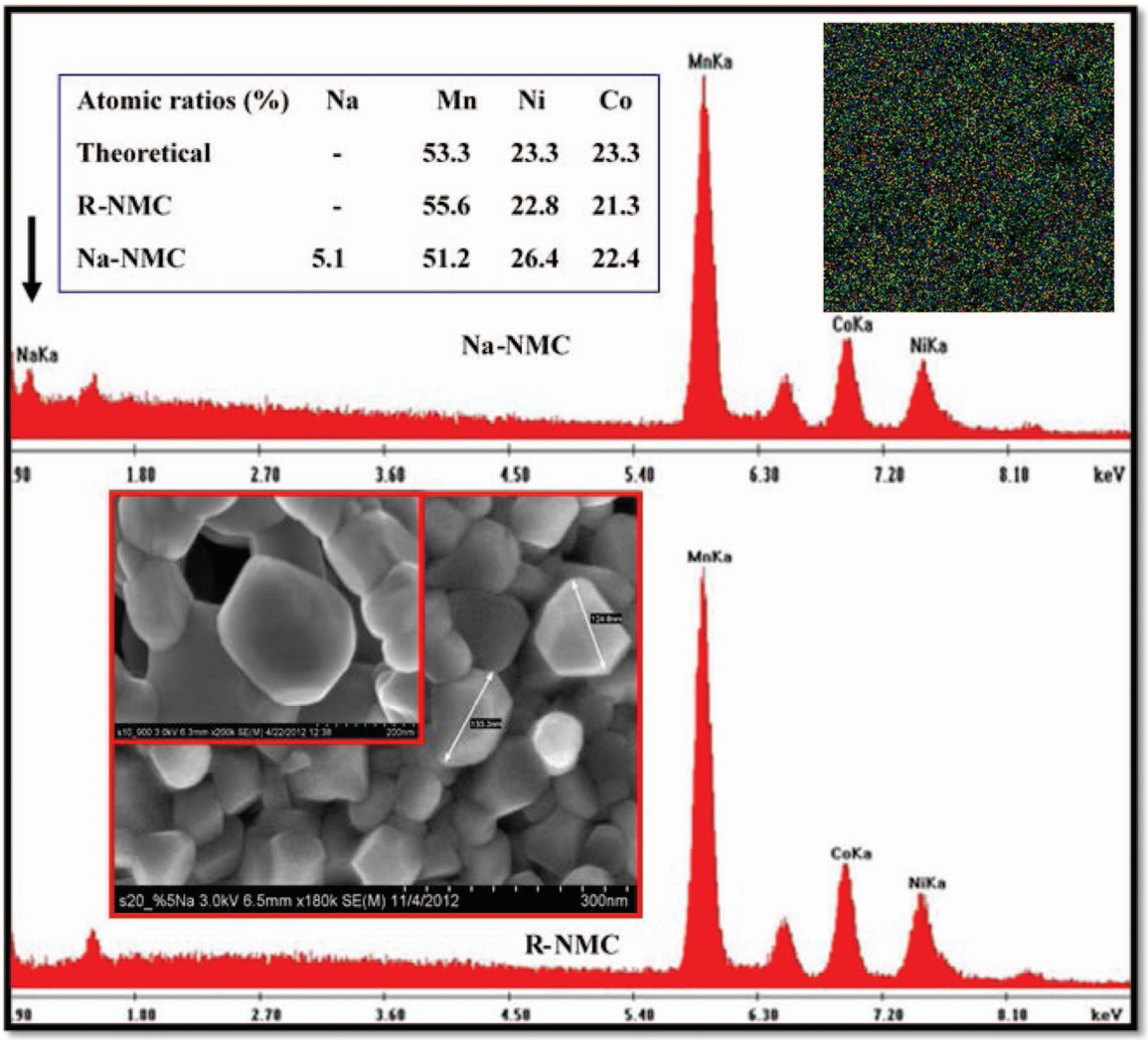

Figure 10. EDAX profiles of Na-NMC doped Li-rich NMC and R-NMC composite cathodes along with the elemental analysis as well as SEM figures. Mapping shows Na-NMC composite cathode where Mn, Ni, Co and Na atoms represented by green, yellow, blue and red colors, respectively.

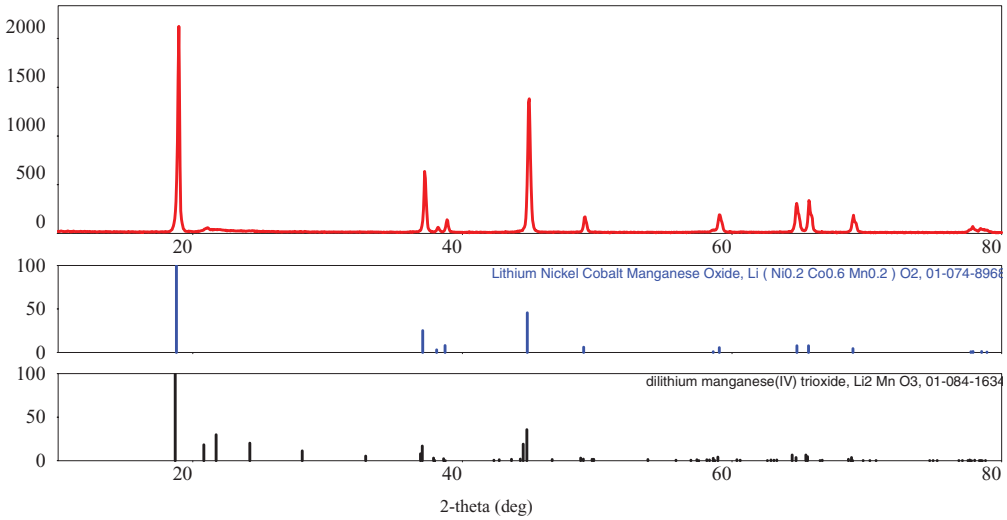

Figure 11. Bragg positions of each reference compounds Li_2MnO_3 and $LiMO_2$ acquired during refinement process with respect to experimental patterns of R-NMC.

Table II. Refined crystal parameters of pristine R-NMC and Na-NMC powders along with Na-NMC powders treated with electrolyte. Targeted space group was selected as R3m.

Compounds	a (A)	b (A)	c (A)	V(A^3)	c/a ratio	Refinement parameters-PDXL software
R-NMC	2.8411	2.8411	**14.1660**	**99.026**	4.9861	**Rwp:13.56, Rp: 9.28, Re: 7.41, S:1.83**
Na-NMC pristine	2.8497	2.8497	**14.2110**	**99.944**	4.9868	**Rwp:7.82, Rp: 5.86, Re: 4.25, S:1.84**
Na-NMC 24h stirred with electrolyte	2.8519	2.8519	**14.2206**	**100.163**	4.9864	**Rwp:7.83, Rp: 5.53, Re: 4.19, S:1.87**
Na-NMC 48h stirred with electrolyte	2.8551	2.8551	**14.2327**	**100.476**	4.9850	**Rwp:7.5, Rp: 5.48, Re: 4.17, S:1.79**

and 48h, the c parameter becomes larger which is similar to the data reported by Ceder et. al. for $NaMnO_2$ compound.[38] They reported that once the Na in $Na_{0.93}MnO_2$ decreased to the composition $Na_{0.70}MnO_2$, c lattice expansion took place as we observed. Similar observations were reported by Delmas et. al. for P2-Na_xCoO_2 compound where they found that expansion in the c direction is greatly affected by the amount of Na.[20] Both Ceder and Delmas obtained materials exhibiting the expansion through electrochemical removal of Na. In our case small amount of Na is being removed chemically. Possible explanation for this lattice expansion can be discussed further. Firstly, Na atoms can occupy two sites in the crystal structure of Na_xCoO_2 as noted by Ceder.[39] These two different site occupations of Na atoms, namely Na(1) and Na(2), have totally different effect on crystal phases. Na(1) atoms share its top and bottom sides with metal oxygen layers, while

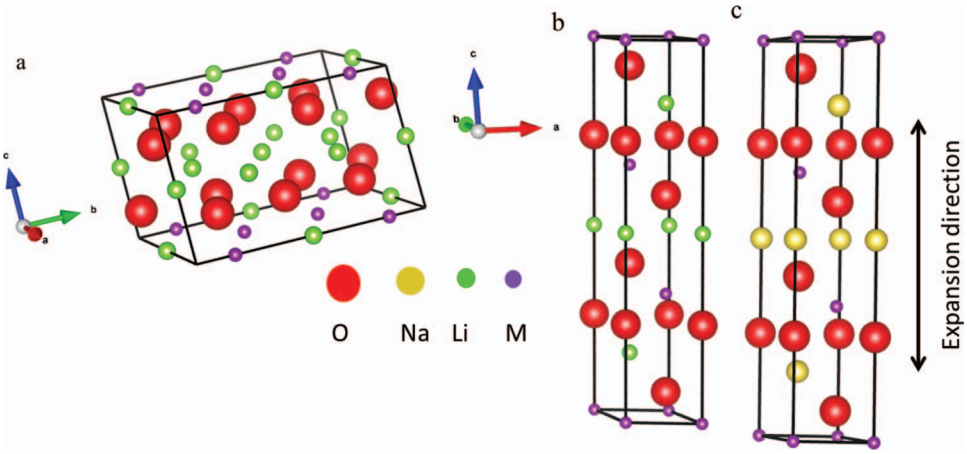

Figure 12. Unit cells of a) Monoclinic (C2/m) Li_2MnO_3 unit cell b) Trigonal (R3m) $LiMO_2$ c) Trigonal (R3m) $NaMO_2$.

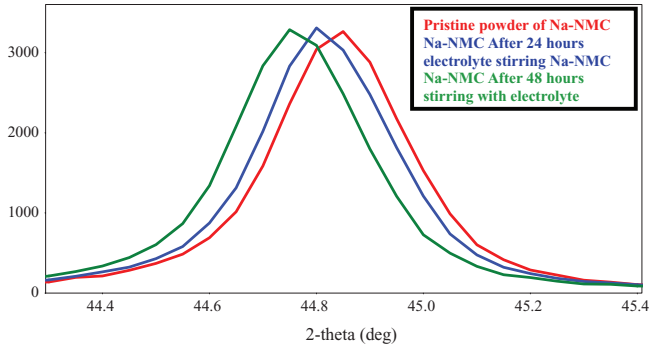

Figure 13. The effect of electrolyte storage on a magnified peak located at around 45 degrees. A clear shift toward lower angle is observed as Na atoms are exchanged by Li atoms present in the electrolyte.

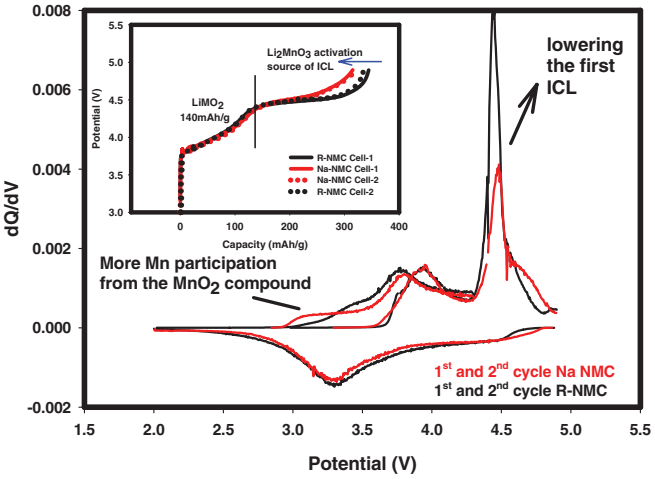

Figure 14. Differential charge and discharge capacities against voltage profiles for both Na-NMC and R-NMC cathodes at 50°C at 1st and 2nd cycling. Inset figure shows first charge process based on galvanostatic data for R-NMC and Na-NMC at room temperature.

Na(2) atoms share its edges with metal oxygen layers.[40] One can surmise that Na(1) atoms are located at sites where they push apart metal oxygen layers thereby creating expansion. Na(1) site occupancy increases when the overall concentration of Na atoms in the metal oxide decreases as shown by Huang.[41]

Another piece of information worth noting is that the c/a ratio is slightly decreasing with time which is probably a sign of metals, perhaps Ni, migration into Li layers. Most probably it is Ni^{3+} which is migrating as this occurs during the first charge. The movement of Ni to Li layer was discussed by several authors for $LiNi_{0.5}Mn_{0.5}O_2$ and $LiNi_{0.85}Mn_{0.15}O_2$.[42–44] Volume expansion mainly by c parameter enlargement can be seen by looking at a specific XRD peak located at around 45 2θ degrees, belonging to (104) plane. Figure 13 shows that the peak around 45 degrees is shifted toward the lower angle which is an indication of volume expansion due to increasing d spacing. This volume expansion and possible transition metal migration, most probably Ni, particularly after the activation of Li_2MnO_3 in the first charge, into Li layers in Na-NMC ultimately facilitate better Ni and Mn (located in MnO_2 layers) redox reactions as supported the XAS data discussed below. Similar to what we observed for this specific peak located at 45 2θ degrees, we found other peaks such as those at 18, 37 and 49 2θ degrees, corresponding to (003), (101) and (015) planes, respectively, showing similar trends – a shift to lower angles-suggesting that this is not just the case for a certain peak but rather a whole crystal structure following the same trend. The cyclic voltammetry data obtained at RT affirms that Mn participation in the MnO_2 layers can be distinguished better with Na doping and likewise, this behavior was observed in the dQ/dV plots derived from the galvanostatic data at 50°C displayed in Figure 14. By looking at both plots in Figure 14, the lower ICL of Na-NMC can be observed readily from the galvanostatic data at RT as well as derivative dQ/dV plots at 50°C. Two different cells corresponding to each material are presented to show reproducibility in the inset of Figure 14. To further elaborate this, the columbic efficiency at RT was calculated based on the first charge and the discharge capacities at C/20 rates. The results show that that R-NMC has 70% columbic efficiency, while Na-NMC displays 82% of columbic efficiency. Both of these observations led us to conclude that Na-NMC has lower irreversible capacity loss (ICL) and better Mn participation than that of R-NMC composite cathode. We like to note that in general, the voltage swifts of the oxidation peaks in CV and dQ/dV plots to lower potentials after the activation of Li_2MnO_3 is attributed to two major reasons: i-) a change in the local geometry of Ni atoms due to their migration to the Li depleted layers in Li_2MnO_3 and ii-) the structural transformation that takes place during the first charge after 4.6 V.[45]

X ray absorption (XAS) is one of the versatile tools to investigate the local coordination environment of a specifically selected atom along with its valence state with high precision. The information gained from XRD data were complemented with XAS which is discussed below. Since Mn K-edge shift is not clear enough to distinguish the valence states[46] due its complex location on both layered structures (R3m and C2/m SG), we performed our first experiments at Ni K-edge where redox couples transit between $2^+/4^+$, thereby it is easy to determine the valence state changes during the first full cycle. The three points selected to investigate the Ni and Mn K-edge shifts were 4.3 V, 4.9 V and 2 V during the first cycle. The first cycle capacity retentions of R-NMC were similar to that of Na-NMC in the disassembled cells. Both charging and discharging rates were set at C/20 in order to allow efficient Li extraction. XANES data at points where XAS data were acquired were consistent with the reported data published elsewhere.[47,48,46] We used NiO as Ni^{2+} reference and $LiNi_{0.85}Co_{0.15}O_2$ as Ni^{3+} reference and the latter was charged to 5.1 V to obtain Ni^{4+} reference as reported by Balasubramanian et al.[7] XANES data of Ni K-edge are plotted in Figure 15 along with the above mentioned reference compounds. Once the Li cell started to charge, the shift toward higher energy is observed due to higher valance state of Ni atoms in both cases as expected. Contrary to some previous reports[49,50,51] that Ni is being oxidized to 4^+ in the lithium rich composite electrode materials, our experiments revealed that the valance state of the Ni ions is slightly below 4^+ at 4.9 V in both Na-NMC and R-NMC electrodes. Similar observations were reported elsewhere.[46,48] At the 4.3 V and 4.9 V charging points, both of the composite cathodes have similar valence states. Nevertheless, at the first discharge end point of 2 V, Ni in Na-NMC has been reduced more compared to the Ni in R-NMC compound as evidenced by having larger crystal volume (Table III) and lower XANES energy (eV) profile (Figure 15) for Na-NMC. Although the reduced state of Ni in Na-NMC is higher than Ni^{2+}, it is more reduced than the Ni present in R-NMC leading to higher discharge capacity. Overall, Ni ions present in the pristine electrodes have an average oxidation state between 2^+ and 3^+ and probably closer to 2^+, while in the charged state at 4.9 V they have an average oxidation state between 3^+ and 4^+ and perhaps closer to 4^+. Traditional Fourier Transforms (FT) EXAFS analysis is applied to the Ni K edge. The best-fit values of the structural parameters are listed in Table III. A representative k^3-weighted experimental data $\chi(k)$ and the corresponding Fourier transforms (FT) of Na-NMC at 4.3 V charged state, together with the fitted data which clearly shows an excellent overlap for the first two shells namely Ni-O and Ni-M (M = Co or Ni) scatterings (not shown here). The coordination number of the first (Ni-O) and second shells (Ni-M, M = Ni or Co) was found to be ~6. These results agree well with the previous studies on the similar compounds.[48] As expected and reported elsewhere,[48] it is obvious from the table that the Ni-O and Ni-M bond distances are decreasing as the electrodes are charged due to higher valance

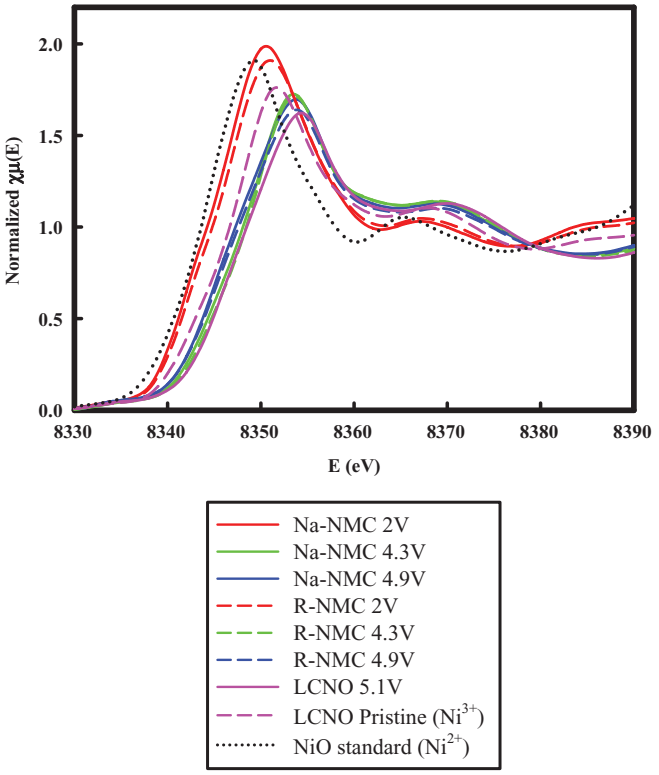

Figure 15. Ni K-Edge XANES data of several samples including reference compounds noted with respect to their potentials in Li cells.

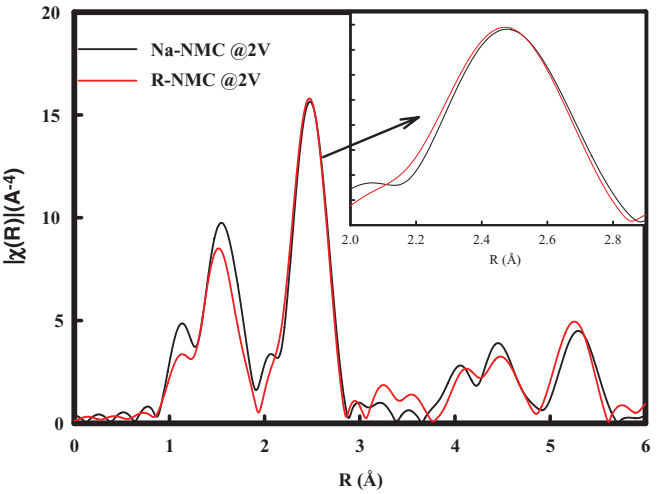

Figure 16. Fourier transforms (FT) of the Ni absorber atom in both Na-NMC and R-NMC at 2 V after the first full cycle.

states, while after the first discharge both Ni-O and Ni-M bonds are increasing due to lower valance state of Ni. Figure 16 displays Fourier transforms (FT) of the Ni in both Na-NMC and R-NMC at 2 V after one single full cycle. From this figure and the corresponding EXAFS fitting results listed in Table III, one can distinguish that Na-NMC has longer Ni-O bond distance than NMC which can be consistently related to the XANES results (Figure 15) where the Ni in Na-NMC is reduced more compared to that in R-NMC. The inset in Figure 16 is the magnified peak located in the second shell attributed to the scattering from the nearest surrounding M, which show that Na-NMC has longer Ni-M bond distance than R-NMC as determined from EXAFS fittings (Table III). The Ni-M-M scattering also shows that in the case of Na-NMC after the activation process and possible ion swapping, some additional TM rearrangements occurs leading to larger crystal volume. Furthermore, the peaks are centered at 5.2 Å (double the Ni-M bond distance), derived from the single and multiple scatterings from the surrounding M farther away. The collinear focusing double and triple scattering from the nearest surrounding M (Ni-M-M)[52] shows a very clear shift in which Na-NMC has larger Ni-M-M bond distance resulting in a larger crystal cage compared to R-NMC. One of the most intriguing results from the EXAFS data is that Na-NMC after the first discharge, when substantial amount of Na is removed, has a larger crystal cage compared to R-NMC which may provide a path for efficient Li transport into and out of the crystal structure. This is perhaps due to metal migration, specifically Ni, in Na-NMC to the Na^+ depleted regions triggered by its exchange with Li^+ in solution during the activation of Li_2MnO_3. Even though Na sites are more favorable for Li ions, based on each metal's radius, Ni^{2+} (0.69A) has the closest radius to the space created by Na^+ removal.

Since we observed a major change in Ni K edge at the first discharge point, 2 V, we also performed Mn K edge experiments to support our observation from CV results of more pronounced Mn participation in Na-NMC than in R-NMC. Figures 17a and 17b display normalized XANES spectrum of the Mn K edge and the Mn K pre-edge, respectively of both compounds along with the spinel reference compound which has 3.5^+ valance state. From this spectrum, one can easily surmise that in both R-NMC and Na-NMC, the valence states are identical at 4.9 V during the first charge and after one full cycle at 2 V. The redox couples for Mn at 4.9 V is believed to be higher than 3.5^+ (closer to 4^+) and at 2 V not too lower than 3.5^+ as in the Mn spinel oxide. However, during the first charge of Na-NMC to 4.3 V, the Mn has significantly higher oxidation state ($>3.5^+$) than in R-NMC. This distinguishable difference in Mn participation is detected during CV cycles at both RT and high temperatures (see Figure 14). The answer to the question of which Mn participation occurs in Na-MNC comes from the elucidation of Mn K pre-edge spectrum which is shown in Figure 17b. Mn K pre-edge regions have been studied and well documented by several groups[33,46] and were associated to electronic excitation of 1s core electrons to unoccupied 3d orbitals in TM ions. This formal electric-dipole transition is forbidden in a normal octahe-

Table III. Ex situ EXAFS fit results for indicated samples collected at three potentials. Experiments performed at Ni K edge. The coordination number (CN), phase-corrected bond length (R), and Debye-Waller factor (σ^2) are shown for each interaction.

Sample	LCNO pristine	LCNO 5.1 V	R-NMC 4.3 V	Na-NMC 4.3 V	R-NMC 4.9 V	Na-NMC 4.9 V	R-NMC 2 V	Na-NMC 2 V
$R_{Ni\text{-}O}$ (Å)	1.952	1.88	1.888	1.893	1.881	1.891	2.005	2.017
$R_{Ni\text{-}Ni/Co}$ (Å)	2.873	2.818	2.823	2.825	2.809	2.82	2.855	2.867
$CN_{Ni\text{-}O}$	5.6	5.8	5.5	5.8	5.7	5.8	6 (fixed)	6.4
$CN_{Ni\text{-}Ni/Co}$	6.5	5.6	6.2	6.7	5.7	6.0	6 (fixed)	6.4
$\sigma_{Ni\text{-}O} \times 10^{-3}$	8.9	3.8	2.5	3.9	4.7	5.4	5.6	5.6
$\sigma_{Ni\text{-}Ni/Co} \times 10^{-3}$	5.5	3.8	4.8	5.3	5.6	5.9	5.6	5.6

*S_0^2 fixed at 0.82 as obtained by fitting the reference iron foil. The Fourier-transformed (FT) EXAFS data were fitted under k^3 weighting, R range 1.00 – 3.16 Å, k range 2.70 – 14.15 $Å^{-1}$. The statistical errors of the least-squares fits were determined by ARTEMIS.

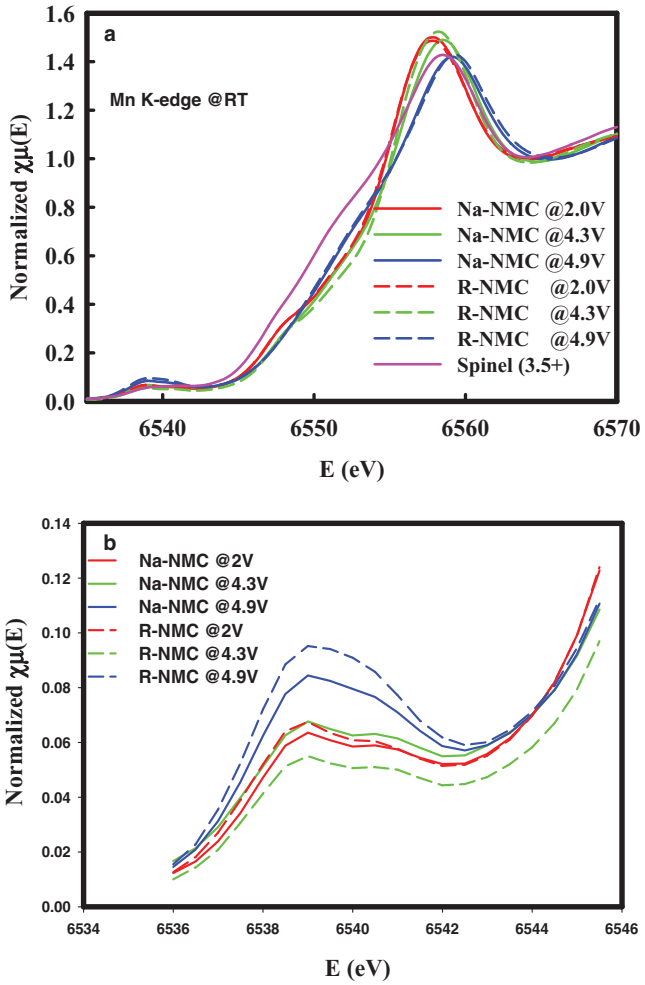

Figure 17. a-) Normalized XANES spectra of Mn K edge at RT and b) Mn K pre-edge spectra of both compounds at various potentials.

dral symmetry. It is well known that these weak peaks are arising from the non-centrosymmetric environment of the distorted 3a sites in the R3m,[46] where transition metals occupy in the space group of $LiMO_2$. In Figure 17b, at the first charge point of 4.9 V and after one full cycle at the 2 V region, Na-NMC compound has less distortion in 3a states in R3m space group of $LiMO_2$ even though they have identical valence states. However, at 4.3 V during the first charge, Na-NMC has higher distortion in 3a sites of $LiMO_2$ which clearly asserts that Mn participation is stimulated by Na doping located in $LiMO_2$ sites which has R3m space group. This information also leads us to conclude that the doped Na is most probably located in $LiMO_2$ portion of the crystal lattice rather than in Li_2MnO_3. We also obtained Co K edge spectrum (not shown here) after one full cycle to determine whether Na-NMC had better Co reduction compared to R-NMC, however the peaks at 2 V have identical profiles indicating that Co redox behavior was not affected by Na doping.

Conclusions

The lithium rich layered composite cathode material $0.3Li_2MnO_3 0.7LiMn_{0.33}Ni_{0.33}Co_{0.33}O_2$ and its 5 wt% Na doped counterpart, $0.3Li_2MnO_3.0.7Li_{0.97}Na_{0.03}Mn_{0.33}Ni_{0.33}Co_{0.33}O_2$, were synthesized through a co-precipitation method. Li cell impedance and dc conductivity of pressed pellets showed that Na substitution improves the electronic conductivity of the Li rich NMC material. High temperature (50°C) impedance tests also revealed less resistance for Na-NMC than for R-NMC although a good fraction of the Na is exchanged with the Li in the electrolyte. This lower impedance translates into better rate capability for Na-NMC. Our electrochemical and structural data indicate that Na plays an important role in improving the electrochemical performance of Li-rich cathode materials studied here. Importantly, Na substitution for Li mitigates the layer to spinel conversion which is a major improvement of this class of cathode materials.

XRD data demonstrated that Na-NMC has larger volume than R-NMC. Although Na is exchanged with Li from solution during cell the activation of Li_2MnO_3 in the first charge, transition metals, most probably Ni^{3+}, migrate to this Na depleted ionic sites in the crystal structure. This process has a stabilizing effect on the crystal structure of the composite material and protects it against conversion to the spinel structure. Charge/discharge cycling at 50°C demonstrated that R-NMC experiences layer to spinel conversion even in the initial cycles whereas Na-NMC has significantly better structural robustness and inhibits the spinel conversion. The dQ/dV plots of the 50°C cycling data of Na-NMC provided evidence for the stabilization of the crystal structure by impeding layered-spinel conversion through preservation of its sloping voltage regions where redox reactions take place. Our XANES and EXAFS data support this conclusion by revealing better Ni reduction for Na-NMC than for R-NMC and greater Ni-O distance at 2 V leading to larger crystal volume. Mn participation during the oxidation of cathodes has been detected via CV. This has been supported by XAS results. The larger crystal lattice of Na-NMC most likely provides better transition metal migration into the Na depleted sites in the Li layers after the activation of Li_2MnO_3 in the first charge. As a future investigation, Na doping will be attempted with other Li rich compounds which are already optimized in terms of capacity and rate capabilities. We believe that Na doping is a simple way to improve the cycle life and rate capabilities of Li rich layered-layered composite cathode materials for Li-ion batteries, and stabilize their structures against the undesirable conversion to the spinel phase.

Acknowledgment

Special thanks to Erik Farquhar for assistance with the XAS experiments conducted at Brookhaven National Lab. This publication was made possible by the Center for Synchrotron Biosciences grant, P30-EB-009998, from the National Institute of Biomedical Imaging and Bioengineering (NIBIB). This work was supported by the Department of Defense.

References

1. J. R. Croy, D. Kim, M. Balasubramanian, K. Gallagher, S.-H. Kang, and M. M. Thackeray, *Journal of The Electrochemical Society*, **159**, A781 (2012).
2. Z. Q. Deng and A. Manthiram, *The Journal of Physical Chemistry C*, **115**, 7097 (2011).
3. Z. Li, N. A. Chernova, J. Feng, S. Upreti, F. Omenya, and M. S. Whittingham, *Journal of The Electrochemical Society*, **159**, A116 (2011).
4. S. K. Martha, J. Nanda, Y. Kim, R. R. Unocic, S. Pannala, and N. J. Dudney, *Journal of Materials Chemistry A*, **1**, 5587 (2013).
5. M. M. Thackeray, C. S. Johnson, J. T. Vaughey, N. Li, and S. A. Hackney, *Journal of Materials Chemistry*, **15**, 2257 (2005).
6. D. Im, J. Kim, J. Yoon, K.-S. Park, Y.-G. Ryu, S. S. Lee, D. J. Lee, and S.-G. Doo, *Electrochemical Society Meeting Abstracts*, **MA2010-01**, 630 (2010).
7. M. Balasubramanian, X. Sun, X. Q. Yang, and J. McBreen, *Journal of The Electrochemical Society*, **147**, 2903 (2000).
8. K. Momma and F. Izumi, *Journal of Applied Crystallography*, **44**, 1272 (2011).
9. Y. Ein-Eli, W. Wen, and S. Mukerjee, *Electrochemical and Solid-State Letters*, **8**, A141 (2005).
10. B. Ravel and M. Newville, *Journal of Synchrotron Radiation*, **12**, 537 (2005).
11. M. Newville, *Journal of Synchrotron Radiation*, **8**, 322 (2001).
12. K. M. Abraham, *Solid State Ionics*, **7**, 199 (1982).
13. D. Kim, S.-H. Kang, M. Slater, S. Rood, J. T. Vaughey, N. Karan, M. Balasubramanian, and C. S. Johnson, *Advanced Energy Materials*, **1**, 333 (2011).
14. A. D. Robertson, A. R. Armstrong, A. J. Paterson, M. J. Duncan, and P. G. Bruce, *Journal of Materials Chemistry*, **13**, 2367 (2003).
15. J. Barker, M. Y. Saidi, and J. L. Swoyer, *Journal of The Electrochemical Society*, **151**, A1670 (2004).
16. S. P. Ong, V. L. Chevrier, G. Hautier, A. Jain, C. Moore, S. Kim, X. Ma, and G. Ceder, *Energy and Environmental Science*, **4**, 3680 (2011).

17. S. Kim, X. Ma, S. P. Ong, and G. Ceder, *Physical Chemistry Chemical Physics*, **14**, 15571 (2012).
18. C. Didier, M. Guignard, C. Denage, O. Szajwaj, S. Ito, I. Saadoune, J. Darriet, and C. Delmas, *Electrochemical and Solid-State Letters*, **14**, A75 (2011).
19. L. A. de Picciotto, M. M. Thackeray, W. I. F. David, P. G. Bruce, and J. B. Goodenough, *Materials Research Bulletin*, **19**, 1497 (1984).
20. D. C. a. C. D. R. Berthelot, *Nature Materials*, **10**, 74 (2010).
21. T. Shibata, W. Kobayashi, and Y. Moritomo, *AIP Advances*, **3**, 032104 (2013).
22. D. Kim, S.-H. Kang, M. Balasubramanian, and C. S. Johnson, *Electrochemistry Communications*, **12**, 1618 (2010).
23. W. He, D. Yuan, J. Qian, X. Ai, H. Yang, and Y. Cao, *Journal of Materials Chemistry A*, **1**, 11397 (2013).
24. F. Amalraj, D. Kovacheva, M. Talianker, L. Zeiri, J. Grinblat, N. Leifer, G. Goobes, B. Markovsky, and D. Aurbach, *Journal of The Electrochemical Society*, **157**, A1121 (2010).
25. C. S. Johnson, N. Li, C. Lefief, J. T. Vaughey, and M. M. Thackeray, *Chemistry of Materials*, **20**, 6095 (2008).
26. L. Xiao, Y. Zhao, Y. Yang, Y. Cao, X. Ai, and H. Yang, *Electrochimica Acta*, **54**, 545 (2008).
27. F. Amalraj, M. Talianker, B. Markovsky, D. Sharon, L. Burlaka, G. Shafir, E. Zinigrad, O. Haik, D. Aurbach, J. Lampert, M. Schulz-Dobrick, and A. Garsuch, *Journal of The Electrochemical Society*, **160**, A324 (2013).
28. J. L. Briant and G. C. Farrington, *Journal of The Electrochemical Society*, **128**, 1830 (1981).
29. M. M. Thackeray, S. H. Kang, C. S. Johnson, J. T. Vaughey, and S. A. Hackney, *Electrochemistry Communications*, **8**, 1531 (2006).
30. D. Kim, J. Gim, J. Lim, S. Park, and J. Kim, *Materials Research Bulletin*, **45**, 252 (2010).
31. Y. Zhao, W. Ren, R. Wu, Y. Yue, and Y. Sun, *J Solid State Electrochem*, **17**, 2259 (2013).
32. N. Li, R. An, Y. Su, F. Wu, L. Bao, L. Chen, Y. Zheng, H. Shou, and S. Chen, *Journal of Materials Chemistry A*, **1**, 9760 (2013).
33. K. Karthikeyan, K. W. Nam, E. Y. Hu, X. Q. Yang, and Y. S. Lee, *Bulletin of the Korean Chemical Society*, **34**, 1995 (2013).
34. M. Y. Son, Y. J. Hong, S. H. Choi, and Y. C. Kang, *Electrochimica Acta*, **103**, 110 (2013).
35. F. Cheng, Y. Xin, J. Chen, L. Lu, X. Zhang, and H. Zhou, *Journal of Materials Chemistry A*, **1**, 5301 (2013).
36. M. Han, T. Sun, P. Y. Tan, X. Chen, O. K. Tan, and M. S. Tse, *RSC Advances* (2013).
37. T. E. Quine, M. J. Duncan, A. R. Armstrong, A. D. Robertson, and P. G. Bruce, *Journal of Materials Chemistry*, **10**, 2838 (2000).
38. X. Ma, H. Chen, and G. Ceder, *Journal of The Electrochemical Society*, **158**, A1307 (2011).
39. Y. S. Meng, Y. Hinuma, and G. Ceder, *The Journal of Chemical Physics*, **128**, 104708 (2008).
40. Y. Hinuma, Y. S. Meng, and G. Ceder, *Physical Review B*, **77**, 224111 (2008).
41. Q. Huang, M. L. Foo, R. A. Pascal Jr., J. W. Lynn, B. H. Toby, T. He, H. W. Zandbergen, and R. J. Cava, *Physical Review B*, **70**, 184110 (2004).
42. B. Xu, D. Qian, Z. Wang, and Y. S. Meng, *Materials Science and Engineering: R: Reports*, **73**, 51 (2012).
43. M. Whittingham, *Chemical Reviews*, **104**, 4271 (2004).
44. J. P. P.-R. C. Julien and A. Momchilov, *New Trends in Intercalation Compounds for Energy Storage*, in, p. 187, Springer (2002).
45. S. H. Kang, P. Kempgens, S. Greenbaum, A. J. Kropf, K. Amine, and M. M. Thackeray, *Journal of Materials Chemistry*, **17**, 2069 (2007).
46. A. Ito, Y. Sato, T. Sanada, M. Hatano, H. Horie, and Y. Ohsawa, *Journal of Power Sources*, **196**, 6828 (2011).
47. N. Yabuuchi, K. Yoshii, S.-T. Myung, I. Nakai, and S. Komaba, *Journal of the American Chemical Society*, **133**, 4404 (2011).
48. J. R. Croy, M. Balasubramanian, D. Kim, S.-H. Kang, and M. M. Thackeray, *Chemistry of Materials*, **23**, 5415 (2011).
49. H. Yu, H. Kim, Y. Wang, P. He, D. Asakura, Y. Nakamura, and H. Zhou, *Physical Chemistry Chemical Physics*, **14**, 6584 (2012).
50. G. Singh, R. Thomas, A. Kumar, and R. S. Katiyar, *Journal of The Electrochemical Society*, **159**, A410 (2012).
51. D. Mohanty, S. Kalnaus, R. A. Meisner, K. J. Rhodes, J. Li, E. A. Payzant, D. L. Wood Iii, and C. Daniel, *Journal of Power Sources*, **229**, 239 (2013).
52. A. I. Frenkel, C. W. Hills, and R. G. Nuzzo, *The Journal of Physical Chemistry B*, **105**, 12689 (2001).